Conclusions

Two distinct types of water molecules were found in both $AlPO_4$-5 and VPI-5. The first corresponds to water molecules undergoing fast isotropic reorientation within the channels and the second to water molecules bound to framework Al. Exchange between the two types has been observed in both materials. In VPI-5, however, this exchange is accompanied by a 3-fold jump indicating a relatively high degree of water ordering within the channel. The order at which these two types of water form is different in both materials. In $AlPO_4$-5, reduction of the water content results in a decrease in the amount of bound water, whereas in VPI-5, the opposite takes place. The presence of the template in $AlPO_4$-5 hinders this exchange.

Sorbed ammonia molecules in VPI-5 are present in three distinct dynamic states, free physisorbed molecules, molecules bound to framework Al and undergoing a rotation about the N-Al axis, and rigid molecules bound to octahedral framework Al. Unlike in the case of water, no exchange between the three states was observed. Although the VPI-5 channel is larger than that of $AlPO_4$-5, the water exhibits a greater degree of order in VPI-5 which reflects the special role it may play in the structure stabilization.

Acknowledgment. This study was made possible by funds granted to D.G. through a fellowship program sponsored by the Charles H. Revson Foundation. We thank K. Zukerman for sample preparation and A. J. Vega and R. Poupko for very helpful discussions. We also thank L. McCusker and co-workers for making the preprint of their work available to us.

Registry No. H_2O, 7732-18-5; NH_3, 7664-41-7.

Hemoglobin R→T Structural Dynamics from Simultaneous Monitoring of Tyrosine and Tryptophan Time-Resolved UV Resonance Raman Signals

Kenton R. Rodgers,[†] Chang Su,[†] Shankar Subramaniam,[‡] and Thomas G. Spiro*,[†]

Contribution from the Department of Chemistry, Princeton University, Princeton, New Jersey 08544, and the Department of Biophysics, University of Illinois, Champaign, Champaign, Illinois 61801. *Received August 27, 1990*

Abstract: High quality ultraviolet resonance Raman (UVRR) spectra with 230-nm excitation are reported for deoxy- and CO-hemoglobin (Hb), and for the HbCO photoproduct, obtained with varying delay between photolysis and probe laser pulses. At 10- to 20-μs delays, the photoproduct-HbCO difference spectrum shows numerous Tyr and Trp difference signals that are indicative of having reached the T state, on the basis of their likeness to the static deoxyHb-HbCO difference spectrum. At earlier delays, the difference signals diminish in intensity and, at submicrosecond delays, are different in shape and frequency. Deconvolution analysis of the W3 band envelope and application of the correlation of W3 frequency with the dihedral angle, $\chi^{2,1}$, to the X-ray coordinates facilitated assignment of these components to the three inequivalent Trp residues, β37, α14, and β15. The Trp β37 assignment was confirmed via the UVRR spectrum of Hb Rothschild, in which Trp β37 is replaced by arginine. The unique environmental sensitivity of the W3 frequency makes this band a particularly rich source of information in the time-resolved UVRR difference spectra, as the different W3 components exhibit quite different temporal evolutions. Changes in these components were evaluated in terms of environmental effects with the aid of excitation profiles (EP's) for the Trp model, 3-methylindole in various solvents. Prompt (30 ns) spectral changes were shown, on the basis of the W3 assignments, to be associated with displacements of the A and E helices on the distal side of the heme pocket in the immediate photoproduct. The 1-μs transient is characterized by an upshifted W17 band, which suggest an intermediate protein structure in which the Trp β37 R-state H-bond is broken. The Tyr ν_{8a} and ν_{8b} (Y8a and Y8b) difference signals are shown to result from small upshifts, with a slight intensity loss in Y8a. These changes are detected in bands that result from six inequivalent but unresolvable Tyr residues. The crystal structures, however, indicate that the H-bonding environments of five of these residues differ insignificantly between the R and T states, and attention naturally focuses on the remaining Tyr α42 residue. This residue resides in the "switch" region of the $\alpha_1\beta_2$ interface, where it forms an H-bond with the carboxylate side chain of Asp β99 only in the T state. Elimination of this H-bond via mutations at Asp β99 is known to reduce cooperativity by destabilizing the T state. It has long been assumed that Tyr α42 is the proton donor to a deprotonated Asp β99 carboxylate in this H-bond. However, this should produce a *downshift* and intensification of Y8b on the basis of other proteins with donor Tyr-carboxylate H-bonds and of UVRR spectra of the Tyr model, *p*-cresol in solvents of varying donor and acceptor numbers. The observed Y8b *upshift* and loss of intensity in Y8a is instead consistent with Tyr α42 *accepting* a proton from a neutral Asp β99 in this critical H-bond. An acceptor H-bond is readily accommodated by the crystallographic coordinates, which show the Asp β99 side chain to be in a solvent-inaccessible hydrophobic environment. Whether this site can actually support protonation of carboxylate at neutral pH is discussed in the context of experimental and computational results.

Introduction

Hemoglobin is widely studied as a paradigm of allostery and of cooperative ligand binding to proteins.[1] The explanation offered 25 years ago by Monod, Wyman, and Changeaux,[2] that cooperativity results from a switch between low- and high-affinity states (T and R, respectively) upon partial ligation of the four heme sites, continues to provide a productive model of Hb function. Under various conditions, however, there are more than two states available to the Hb molecule.[3-5] The T and R states have been

* Author to whom correspondence should be addressed.
[†] Princeton University.
[‡] University of Illinois.

(1) Perutz, M. F. *Annu. Rev. Biochem.* **1979**, *48*, 327.
(2) Monod, J. L.; Wyman, J.; Changeaux, J. P. *J. Mol. Biol.* **1965**, *12*, 88.
(3) Ackers, G. K.; Smith, F. R. *Annu. Rev. Biophys. Chem.* **1987**, *16*, 583.
(4) Viggiano, G.; Ho, C. *Proc. Natl. Acad. Sci. U.S.A.* **1979**, *76*, 3673.

0002-7863/92/1514-3697$03.00/0

associated with the differing quaternary structures of deoxy- and oxyHb,[6,7] which have been studied in great detail. Attention currently focuses on the molecular mechanism of the quaternary rearrangement, which is best studied by kinetic methods. The heme–CO adduct of Hb has a high quantum yield for CO photolysis and the ejection of CO is essentially instantaneous (relative to the width of a nanosecond pulse) upon absorption of a photon of light. Subsequent events have been investigated by measuring the rebinding of ligand, or by studying time-resolved spectra of the deligated molecules. Rebinding occurs via picosecond and nanosecond first-order processes (geminate)[8,9] from within the heme pocket and via slower second-order processes[9,10] from outside the protein. Gibson and co-workers discovered a transition from fast to slow second-order rebinding, with a time constant of ~20 μs,[10] and attributed it to the R→T quaternary rearrangement of fully deligated Hb molecules. This is also the time constant found for the final change in the deoxy-heme absorption spectrum following HbCO photolysis; preceding changes were observed with ~0.1- and ~1.0-μs time constants and were attributed to tertiary changes prior to the quaternary rearrangement.[9]

Structural inferences about these kinetic steps have been derived from resonance Raman (RR) spectroscopy.[11] Molecular tension in the T state is directly observed by the lower stretching frequency, 215 cm^{-1} (actually a weighted average between quite different α and β chain frequencies),[12,13] of the bond between the Fe atom and the imidazole side chain of the proximal histidine residue relative to the 222-cm^{-1} band in the deoxyHb R state. The latter value has been inferred from chemically modified or mutant Hb's in which the T state is destabilized,[14] and has been confirmed in native Hb A by kinetic methods.[15] When monitored with 25-ps[16] or 10-ns[17] photolyzing pulses, the Fe–His frequency is appreciably high, 230 cm^{-1}, and relaxes on the microsecond time scale.[18] Likewise, several high-frequency porphyrin vibrational modes, which are known to be sensitive to the porphyrin core size,[19] show detectable downshifts, relative to equilibrium deoxyHb, when monitored during 20-ps[20] or 7-ns[21] photolyzing pulses. The downshifts have been interpreted as arising from partial restraint of the out-of-plane displacement of the Fe atom, resulting in a slightly expanded core at early times.[21] These studies suggest that forces generated against the protein by the excursion of the Fe atom out of the heme plane following CO ejection result in a compressed Fe–His bond and a pause in the Fe displacement. These forces are then relaxed via protein motions leading to the quaternary switch.

It has recently become possible to probe parts of the protein other than the heme group via ultraviolet RR spectroscopy.[22-27] Excitation at wavelengths below 250 nm results in strong enhancement of aromatic residue vibrational modes with little or no interference from the heme group. In a preliminary communication[28] we reported R→T difference RR features for both tyrosine (Tyr) and tryptophan (Trp) residues, recorded simultaneously with 230-nm excitation. These signals were found to appear ~20 μs after photolysis of the HbCO and provide the first direct structural evidence that the quaternary rearrangement does occur on this time scale. The signals were suggested to arise from residues at the $\alpha_1\beta_2$ interface, Tyr α42 and Trp β37, whose H-bonding status is altered in the R→T transition. Moreover, an altered signal was observed for Trp but not for Tyr at 10 μs, prior to the development of the final difference signals, suggesting an intermediate step in the rearrangement. Subsequently, Kaminaka and co-workers[29] published results of a similar pulse–probe UVRR study but using 218-nm excitation, where Trp and Phe residues dominate the RR spectrum. They reported a 20-μs shift in the Trp 880-cm^{-1} band, which is known to be sensitive to H-bonding, and a simultaneous intensity change in the 1000-cm^{-1} region where Phe and Trp bands overlap. Thus, both studies support a 20-μs R→T switch for deligated Hb, although Kaminaka and co-workers did not detect an intermediate Trp signal at 10 μs.

In this paper we present new and higher quality 230-nm excited transient UVRR spectra of photolyzed HbCO, and an analysis of the results on the basis of model compound studies and the time evolution of the UVRR difference features, aimed at elucidating the structural basis of the Hb signals.

Experimental Methods

Hb A was prepared from fresh human blood by standard procedures.[30] The red blood cells were separated by centrifugation in NaCl solution (9 g/L) and subsequently disrupted by dilution in distilled water. Membrane fragments were centrifuged out and the oxyHb supernate was passed through a deionizing column. The protein was stored frozen at 77 K as the CO derivative. Solutions of 0.25 mM deoxyHb were generated in 50 mM phosphate buffer (0.2 M in $NaClO_4$ as a frequency and intensity standard) at pH 7.4 by irradiating the deoxygenated solution with visible light at 4 °C. At 0.25 mM, the fraction of dimeric Hb is negligible for deoxyHb and only ~6% for oxyHb and HbCO.[31] OxyHb was prepared by exposing the deoxyHb solution to atmospheric O_2 followed by 1 atm O_2 pressure. Absorption spectra[30] were used as criteria for purity.

The UVRR spectrometer is comprised of a XeCl excimer-pumped dye laser, a 1.25-m single spectrograph equipped with a 3600 groove/mm holographic grating, and an intensified diode array detector. The 308-nm XeCl excimer laser was run at 300 Hz to pump coumarin 460 laser dye. The 460-nm dye laser fundamental was frequency doubled with a BBO1 crystal to generate 230-nm pulses of 5-ns fwhm. This system was operated to produce 0.25-mW average power focused to a 100-μm diameter spot at the sample. These conditions correspond to a peak power of 2 × 10^6 W/cm^2 or 10 mJ/pulse·cm^2 (or 1 μJ/pulse). The scattered photons were collected with a Cassegrain mirror and focused onto the entrance slit (150 μm) of the spectrograph. The first order of the dispersed light was imaged on the detector to give a 900-cm^{-1} spectral window with 230-nm excitation.

Sample volumes were 0.5 mL and were contained in a Suprasil quartz NMR tube. The tube was spun at approximately 10 Hz, using a highly centric spinner, around a stationary helical stirring wire. This device insures thorough but gentle mixing of the sample during data collection.

(5) Simolo, K.; Stuckey, G.; Chen, S.; Beiley, M.; Scholes, C.; McLendon, G. *J. Am. Chem. Soc.* **1985**, *107*, 2865.
(6) Baldwin, J.; Chothia, C. *J. Mol. Biol.* **1979**, *129*, 175.
(7) Fermi, G.; Perutz, M. F. *Atlas of Molecular Structures in Biology. 2. Haemoglobin and Myoglobin*; Clarendon Press: Oxford, 1981.
(8) Friedman, J. M.; Rousseau, D. L.; Ondrias, M. R. *Annu. Rev. Phys. Chem.* **1982**, *33*, 471.
(9) Hofrichter, J.; Sommer, J. H.; Henry, E. R.; Eaton, W. A. *Proc. Natl. Acad. Sci. U.S.A.* **1983**, *80*, 2235.
(10) (a) Sawicki, C.; Gibson, Q. H. *J. Biol. Chem.* **1976**, *251*, 1533. (b) Sawicki, C.; Gibson, Q. H. *J. Biol. Chem.* **1979**, *254*, 4058.
(11) Spiro, T. G.; Smulevich, G.; Su, C. *Biochemistry* **1990**, in press.
(12) Kitagawa, T.; Nagai, K.; Tsubaki, M. *FEBS Lett.* **1979**, *104*, 376.
(13) Ondrias, M. R.; Rousseau, D. L.; Kitagawa, T.; Ikeda, M.; Inbushi, T.; Yonetani, T. *J. Biol. Chem.* **1982**, *257*, 8766.
(14) Nagai, K.; Kitagawa, T.; Morimoto, H. *J. Mol. Biol.* **1980**, *136*, 271.
(15) Stein, P.; Terner, J.; Spiro, T. G. *J. Phys. Chem.* **1982**, *86*, 168.
(16) Findsen, E. W.; Friedman, J. M.; Ondrias, M. R.; Simon, S. R. *Science* **1985**, *229*, 661.
(17) Friedman, J. M.; Rousseau, D. L.; Ondrias, M. R.; Stepnoski, R. A. *Science* **1982**, *218*, 1244.
(18) Scott, T. W.; Friedman, J. M. *J. Am. Chem. Soc.* **1984**, *106*, 5677.
(19) Parthasarathi, N.; Hansen, C.; Yamaguchi, S.; Spiro, T. G. *J. Am. Chem. Soc.* **1987**, *109*, 3865.
(20) Terner, J.; Stong, J. D.; Spiro, T. G.; Nagumo, M.; Nicol, M.; El-Sayed, M. A. *Proc. Natl. Acad. Sci. U.S.A.* **1981**, *78*, 1313.
(21) Dasgupta, S.; Spiro, T. G. *Biochemistry* **1986**, *25*, 5941.
(22) Hudson, B. S.; Mayne, L. C. In *Biological Applications of Raman Spectroscopy*; Spiro, T. G., Ed.; John Wiley: New York, 1987; Vol. 2, Chapter 4.
(23) Harada, I.; Takeuchi, H. In *Advances in Infrared and Raman Spectroscopy*; Clark, R. J. H., Hester, R. E., Eds.; John Wiley: New York, 1986; Vol. 13, Chapter 3.
(24) Asher, S. A.; Johnson, C. R.; Murtaugh, J. *Rev. Sci. Instrum.* **1983**, *54*, 1657.
(25) Copeland, R. A.; Spiro, T. G. *Biochemistry* **1985**, *24*, 4960.
(26) El-Antri, S.; Sire, O.; Alpert, B.; Turpin, P.-Y.; Chinsky, L. *Chem. Phys. Lett.* **1989**, *164*, 45.
(27) Liu, G.-Y.; Grygon, C. A.; Spiro, T. G. *Biochemistry* **1989**, *28*, 5046.
(28) Su, C.; Park, Y. D.; Liu, G.-Y.; Spiro, T. G. *J. Am. Chem. Soc.* **1989**, *111*, 3457.
(29) Kaminaka, S.; Ogura, T.; Kitagawa, T. *J. Am. Chem. Soc.* **1990**, *112*, 23.
(30) (a) Antonini, E.; Brunori, M. In *Hemoglobin and Myoglobin in Their Reactions With Ligands*; Elsevier: New York, 1971; pp 2–4. (b) Reference 30a, pp 18–25.
(31) Elbaum, D.; Herskovits, T. T. *Biochemistry* **1974**, *13*, 1268.

The desired atmosphere was maintained by delivering the appropriate gas or gas mixture (saturated with H_2O) into the NMR tube through a thin stainless steel tube and flowing the gas over the solution. Such a sample could be kept in the laser beam for up to 7 h with no apparent degradation as evidenced by the absence of a change in the visible spectrum, by the fact that there was no precipitate visible in the solution, and by the ability to subtract separate spectra acquired from the same sample without seeing difference features. Spectral acquisitions were carried out in 1-h increments. Each final spectrum was comprised of three to six co-added 1-h spectra. Before co-adding the spectra, each one was subtracted from the first spectrum taken from a given sample. If difference features were observed, the spectrum was discarded. The spectral intensities were normalized by adjusting the heights of the perchlorate bands at 934 cm^{-1} to unity in the deoxyHb and HbCO spectra. The normalized spectra of HbCO or HbCO photoproduct were subtracted from that of deoxyHb to give difference spectra whose absolute intensities were directly comparable with each other and with the parent spectra.

The time-resolved spectra were acquired via a pump–probe experiment wherein two XeCl excimer-pumped dye lasers were used. The pump laser was tuned to the 419-nm HbCO Soret absorption band to achieve maximum photolysis yield with a minimum of laser power (pump laser pulse duration was 7 ns). The probe excitation wavelength was 230 nm as described above. The pump and probe beams were overlapped with a dichroic beam splitter that reflects 419 nm and transmits 230 nm. The pump and probe spot sizes were independently adjustable with a telescope placed in the pump beam before the dichroic beam splitter. The pump spot was adjusted to twice the diameter (200 μm) of the probe spot. The spatial overlap of the pump and probe beams was "fine tuned" by maximizing the UV scattering at 230 nm, then maximizing the Raman signal from the scattering of the 419-nm light by independently adjusting the position of the pump spot on the sample. The HbCO was completely photolyzed, as judged by the intensity ratio of the ν_4[46] heme RR bands characteristic of deoxy- and CO-hemes. The necessary pump power was empirically determined by increasing the 419-nm power until the ratio of the deoxy-Hb and HbCO ν_4 band intensities no longer changed. This criterion was met at 15 mW and the average power during the pump–probe experiments was 20 mW.

Time delays between the pump and probe laser pulses were generated by using the pump laser to trigger an electronic delay box, which in turn generated a TTL pulse delayed in time to externally trigger the probe laser. The delay between the pump and probe pulses was monitored with a fast photodiode and an oscilloscope. After the excimer lasers reached thermal equilibrium at 300 Hz, there was no significant timing drift in the firing of the lasers on the time scale of the microsecond delays in these experiments.

Acquisition of time-resolved UVRR Hb spectra was carried out using an interleaving scheme wherein a number of samples contributed a 1-h spectrum at each time delay used in the experiment. The first delay for a given sample was the second delay for the previous sample, and the last delay was the first delay of the previous sample. The number of samples used in the experiment was equal to the number of delay times. Hence, any systematic errors in the execution of the experiment should be equally distributed over all of the spectra.

The Hb samples were handled as described for the static differencing experiments above, except that the atmosphere over the samples was 10% CO in N_2. This atmosphere was necessary to reduce the rate of second-order heme–CO recombination to a point where it was not competitive with the dynamic quaternary processes of the protein.[10] The spectra were calibrated against ethanol and acetone as secondary frequency standards. The solvent spectra obtained with visible excitation were meticulously calibrated versus emission lamp lines.

The UVRR apparatus employed for the model compound studies is described elsewhere.[32] Excitation was provided by a 229-nm pulsed (7 nm, 10 Hz) laser beam, generated by coherent H_2 Raman shifting the second harmonic (532 nm) of a 10-Hz Nd:YAG laser. The beam was focused on the front face of a free flowing stream of sample solution, and the scattered photons were collected as described above. The monochromator was operated in the second order with a 2400 groove/mm grating and in the scanning mode. The Raman scattered light was detected with a solar blind PMT equipped with a gated integrator.

Results

A. Static Difference Spectrum. Figure 1 compares 230-nm excited UVRR spectra of HbCO and deoxyHb from 850 cm^{-1} to 1730 cm^{-1} and the deoxyHb–HbCO difference spectrum. The 934-cm^{-1} ClO_4^- band was used to normalize the spectra for subtraction as described in the Experimental Section. These spectra cover a broader spectral range and are of higher quality than those that we reported earlier,[28] thanks to the low peak power and high average power provided by the excimer-pumped dye laser and to improvements in sample handling technique. Our method of gently stirring the protein solution with a small (ϕ = 4 mm) meniscus, along with the stable laser spot image produced by centric spinning of the sample tube, permitted exploitation of the data collection advantages of the diode array spectrograph. The spectra in Figure 1 contain several bands which arise from tryptophan (Trp) or tyrosine (Tyr) residues. The Trp bands, labeled W_i, are assigned according to the scheme of Harada and co-workers,[23] whereas the Tyr band assignments (Y_i) have been discussed by Rava and Spiro.[23] Several weak bands in the spectra have not yet been identified; however, they do not contribute significantly to the difference spectrum.

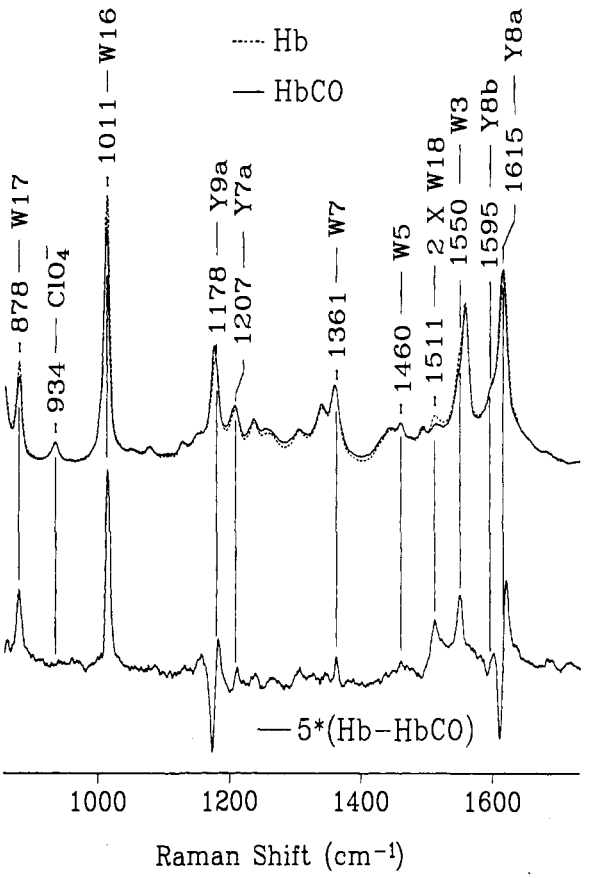

Figure 1. 230-nm excited UVRR spectra of deoxyHb (dashed line) and HbCO (solid line). The difference spectrum (deoxyHb–HbCO) is multiplied by a y-scale factor of 5. For bands that exhibit a shift between the R- and T-state spectra, the frequency marks the inflection point of the difference feature. For bands that only show an intensity change, the frequency labels the peak maximum.

The difference spectrum in Figure 1 is also observed in solutions buffered with Tris at pH 7.4 and is, therefore, not measurably affected by buffering in phosphate versus Tris. Song and Asher report that SO_4^{2-} and ClO_4^- perturb the absorption spectrum of *metHb* and suppress the R→T transition of metHbF in the presence of IHP.[33] They advocated SeO_4^{2-} as a nonperturbing

(32) Fodor, S. P. A.; Rava, R.; Copeland, R. A.; Spiro, T. G. *J. Raman Spectrosc.* **1986**, *17*, 471.

(33) Song, S.; Asher, S. A. *Biochemistry* **1991**, *30*, 1199.
(34) Su, C.; Wang, Y.; Spiro, T. G. *J. Raman Spectrosc.* **1990**, *21*, 435.
(35) Fodor, S. P. A.; Copeland, R. A.; Grygon, C. A.; Spiro, T. G. *J. Am. Chem. Soc.* **1989**, *111*, 5509.
(36) Sharma, V. S.; Newton, G. L.; Ranney, H. M.; Ahmed, F.; Harris, J. W.; Danish, E. *J. Mol. Biol.* **1980**, *144*, 267.
(37) Demchenko, A. P. In *Ultraviolet Spectroscopy of Proteins*; Springer-Verlag: Berlin, 1987; pp 80–86.
(38) Hildebrandt, P.; Copeland, R. A.; Spiro, T. G.; Otlewski, J.; Laskowski, M.; Prendergast, F. G. *Biochemistry* **1988**, *27*, 5426.

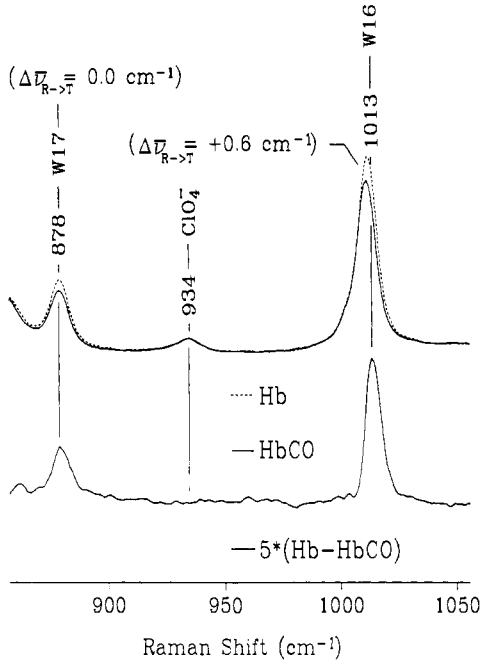

Figure 2. Expansion of the 850-cm^{-1} to 1060-cm^{-1} region of the spectra in Figure 1. The frequency differences, $\Delta\nu_{R\rightarrow T}$, were obtained directly from the band maxima in the R- and T-state spectra.

internal standard. We obtained the same Hb–HbCO difference spectrum with SeO_4^{2-} as with ClO_4^-, but chose the latter because the 834-cm^{-1} SeO_4^{2-} band is close to the Trp W17 band and lies outside of our desired spectral window. It is possible that ClO_4^- perturbs the metHb absorption spectrum by competing with OH_2 for the open Fe(III) coordination site. It is important to note that we use native (ferrous) HbA in our UVRR experiments, and neither OH_2 nor anions bind to the Fe(II) site of native Hb or HbCO. We note in addition that $NaClO_4$ from commercial sources is often contaminated with Cl^-, which would also be expected to interfere with interpretations of ferric heme absorption spectra. The $NaClO_4$ used in our experiments was twice recrystallized before adding it to the Hb samples.

1. Trp Static Difference Features. All of the Trp and Tyr bands in our spectral window give rise to difference features. The difference bands reflect intensity changes and/or frequency shifts. All Trp bands show greater intensity for deoxyHb than for HbCO (Figure 1), whereas the strong Y8a and Y9a bands show lower intensity, although the difference features exhibit sigmoidal character due to frequency shifts. Figure 2 shows an expanded view of the 850–1050-cm^{-1} region of the spectra. The intense W16 band is stronger in deoxyHb and also shifts up detectably, by 0.6 cm^{-1}. (Frequency shifts were determined directly from the peak positions in the two spectra.) Kaminaka et al.[29] likewise found an intensity increase for this band, although the effect is less clear at their excitation wavelength (217.8 nm), as the overlapping 1003-cm^{-1} band of Phe is of comparable intensity. With 230-nm excitation, the Phe contribution in this region is relatively small and the Trp changes are quite clear.[28] The W17 band at 878 cm^{-1} likewise intensifies in our spectra, but it experiences no detectable frequency shift. This is a surprising result, as the W17 frequency is known to be sensitive to H-bonding[23] and the Trp residues experience H-bonding changes between the R and T states (vide infra). Kaminaka et al.[29] do report a 5-cm^{-1} upshift in time-resolved HbCO photoproduct spectra, and also upon converting

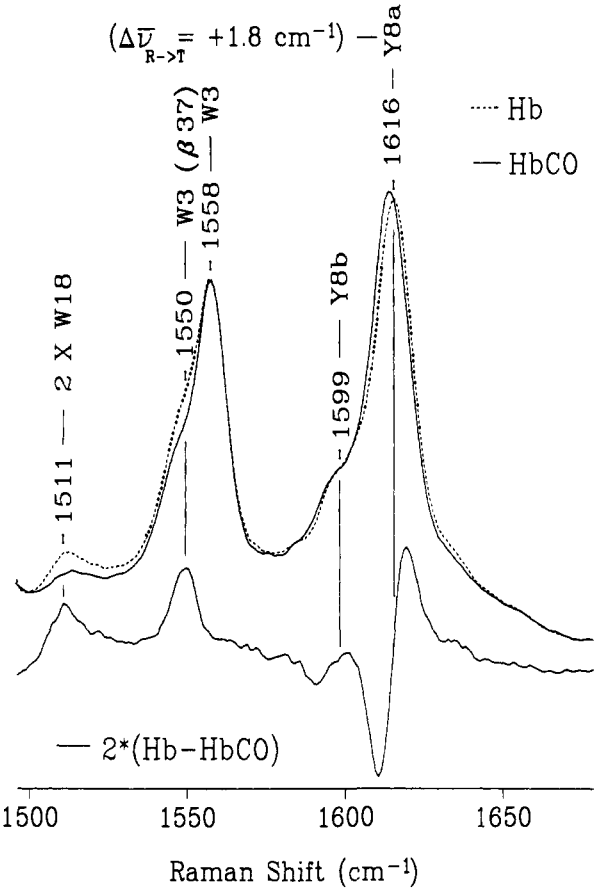

Figure 3. Expansion of the 1490-cm^{-1} to 1680-cm^{-1} region of the spectra in Figure 1. $\Delta\nu_{R\rightarrow T}$ for Y8a was obtained as described for Figure 2, but the difference spectrum is only multiplied by a factor of 2.

metHbF from the R to the T state with IHP. It is possible that compensating changes among the different Trp residues produce different net frequency shifts at 230 nm and 217.8 nm because of excitation profile differences. Further studies are necessary to evaluate this possibility.

For the present study, the most informative spectral region is between 1500 and 1700 cm^{-1}. An expanded view of this region is shown in Figure 3. The prominent features are the Tyr Y8a/Y8b and the Trp W3 envelopes. In addition, a weak band at 1511 cm^{-1} is identified as the overtone of the Trp W18 mode[23] at 763 cm^{-1}, which is strongly enhanced at 230 nm.[32] Like the overtone, the fundamental band is stronger for deoxyHb than for HbCO (data not shown). A band near 1511 cm^{-1} has also been identified with tyrosyl radical, which can be generated transiently at sufficiently high peak laser power.[43] However, in our spectra the 1511-cm^{-1} band intensity is independent of laser power. This is demonstrated by the spectra in Figure 4, wherein, apart from decreased S/N, the spectrum of HbCO is unaltered when the average laser power is decreased from 0.25 to 0.025 mW. This corresponds to a 10-fold decrease in the peak pulse power, as the laser repetition rate was the same (300 Hz) for the two spectra. The featureless difference spectrum means that the spectra are neither subject to ground state depletion of the aromatic residues, nor to photoproduct formation.

The Trp W3 band is unique among the bands in Figure 1, as the Trp environmental heterogeneity is manifested in resolvable spectral heterogeneity (see Figure 3). The Trp W3 band clearly has a low-frequency shoulder, whose intensification in deoxyHb gives rise to the 1550-cm^{-1} difference band. This shoulder arises from the Trp β37 residues, as revealed by the UVRR spectrum of Hb Rothschild (Figure 5), a natural Hb mutant in which Trp

(39) (a) Arnett, E. M.; Jorres, C.; Mitchell, E.; Murty, T. S. S. R.; Gorrie, T. M.; von Schleyer, P. R. *J. Am. Chem. Soc.* **1970**, *92*, 2365. (b) Thijs, R.; Zeegers-Huyskens, Th. *Spectrochim. Acta, Part A* **1984**, *40A*, 1057. (c) Joesten, M. D.; Drago, R. S. *J. Am. Chem. Soc.* **1962**, *84*, 2696.

(40) Ito, M. *J. Mol. Spectrosc.* **1960**, *4*, 125.

(41) *Dictionary of Organic Compounds*, 5th ed.; Chapman & Hall: London, 1982.

(42) Dudik, J. M.; Johnson, C. R.; Asher, S. A. *J. Chem. Phys.* **1985**, *82*, 1732.

(43) Asher, S. A.; Ludwig, M.; Johnson, C. R. *J. Am. Chem. Soc.* **1986**, *108*, 3186.

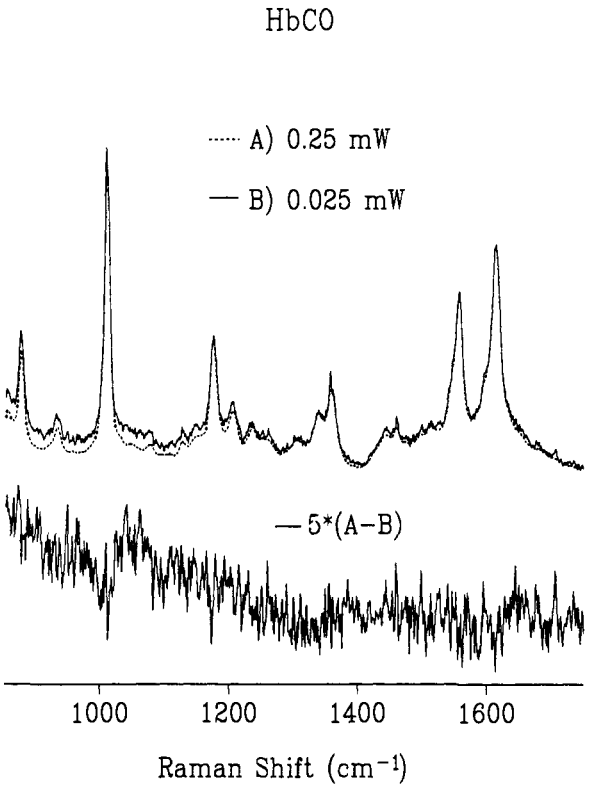

Figure 4. 230-nm excited UVRR spectra of HbCO with 0.25 mW (dashed line) and 0.025 mW (solid line) of average power. The difference spectrum is multiplied by 5. Peak powers are 2 MW/cm^2 and 200 kW/cm^2, respectively.

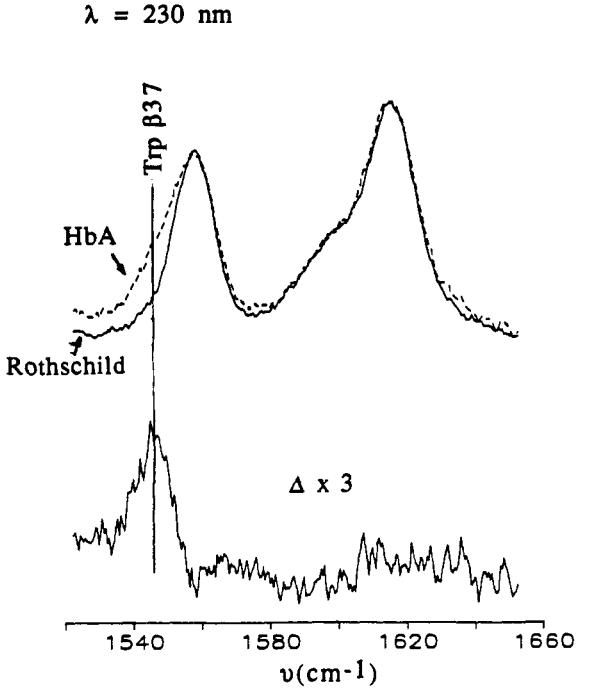

Figure 5. 230-nm excited UVRR spectra in the W3 and Y8a/Y8b region for the O_2 adducts of Hb A (dashed line) and Hb Rothschild (solid line). The difference, shown with 3× y-scale expansion, reveals the 1546-cm^{-1} band attributed to W3 of Trp β37, which is replaced by Arg in Hb Rothschild.

β37 is replaced by arginine.[36] The Hb Rothschild W3 envelope lacks the low-frequency shoulder, and when its spectrum is subtracted from that of Hb A (both in the oxy- form) a difference band at 1546 cm^{-1} is clearly revealed.

The high quality data in Figure 3 support reliable curve-fitting analysis of the W3 envelope. Satisfactory fits to the data were obtained using two bands with 50% Lorentzian and 50% Gaussian line shapes. The Gaussian contribution to the line shape likely arises from the "blooming" effect of the intensified diode array detector. Figure 6 shows the excellent fits to the data obtained by this procedure for HbCO, deoxyHb, and two phototransients, which are discussed below. The difference signals, shown at 3× actual intensity, are fit to within experimental uncertainty by the curve-fitted bands. The frequencies, widths, and areas of the fitted bands are listed in Table I. The lower-frequency band at ~1548 cm^{-1} is assigned to Trp β37, and the higher-frequency band (~1558 cm^{-1}), which has about twice as much intensity, is attributed to overlapping contributions from the remaining Trp residues, α14 and β15. Their contributions cannot be resolved by curve fitting. Moreover, the fact that the 1558-cm^{-1} band is narrower than the 1548-cm^{-1} band, and that it is as narrow as the ν_3 band of the model compound 3-methylindole (3-MeIn) in various solvents (Table III, see below), indicates that the Trp α14 and β15 W3 bands really do fall at essentially the same frequency.

Table I. W3 Spectral Parameters Obtained from Deconvolution of 230 nm Excited UVRR Spectra in the W3 Region

assignment	frequency (cm^{-1})	fwhm (cm^{-1})	area[a]
	HbCO		
Trp β37	1547.1	13.0	31.2
Trp α14/β15	1557.9	10.6	65.7
	30 ns		
Trp β37	1547.4	12.6	30.2
Trp α14/β15	1558.6	10.6	65.7
	1 μs		
Trp β37	1547.5	13.0	33.8
Trp α14/β15	1558.6	10.6	65.7
	5 μs		
Trp β37	1547.8	13.9	36.1
Trp α14/β15	1558.6	10.5	61.9
	10 μs		
Trp β37	1547.7	13.8	40.0
Trp α14/β15	1558.5	10.7	64.2
	20 μs		
Trp β37	1547.8	13.3	37.2
Trp α14/β15	1558.6	10.6	64.7
	DeoxyHb		
Trp β37	1548.2	13.8	42.8
Trp α14/β15	1558.3	10.5	63.0

[a] Areas were calculated by multiplying the fwhm by the peak height, which is given in multiples of the reference (ClO_4^-) peak height.

On the basis of this deconvolution we conclude that the Trp β37 W3 band is 1.1 cm^{-1} higher in deoxyHb than in HbCO, and has 37% greater intensity. These changes are the principal contributors to the W3 difference signal. In contrast, the W3 band that arises from Trp α14 and β15 shows essentially no intensity change and shifts up by only 0.4 cm^{-1} in deoxyHb.

2. Tyr Static Difference Features. The Tyr Y8a and Y8b bands also give rise to strong difference signals (Figure 3). These bands arise from six symmetry-related pairs of Tyr residues, but show no apparent spectral inhomogeneity. There are apparent upshifts of ~1 cm^{-1} and 1.8 cm^{-1} for Y8b and Y8a, respectively, in deoxyHb. These represent aggregate changes for the six Tyr residues. We considered the possibility that other aromatic residues could contribute to these changes, as Phe ν_{8a} and ν_{8b} bands as well as the Trp W1 and W2 bands fall in this region of the spectrum. In Figure 7 we compare the integrated intensity of the 1615/1600-cm^{-1} RR band envelope (measured in a separate experiment against sulfate as an internal standard[35]) as a function of excitation wavelength, along with the intensities expected[34] for the $\nu_{8a} + \nu_{8b}$ of aqueous Phe and Tyr, and the W1 and W2 bands of aqueous Trp, if these chromophores were present at the same molar concentration as in oxyHb. The total intensity expected for the aromatic residues, plotted as "Σ aromatics", tracks that of the oxyHb band envelope quite well, except at 209 nm, where the intensity is dominated by Phe. An environmental effect on the

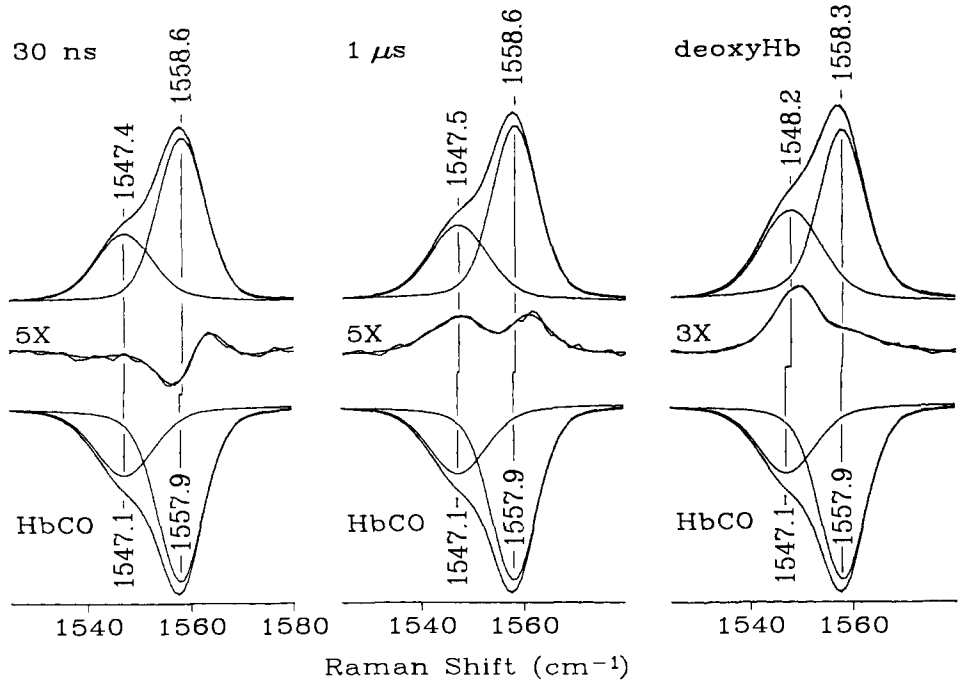

Figure 6. Band deconvolution of the W3 region for HbCO (bottom), deoxy Hb (top right), and the 30-ns and 1-μs phototransients (top left and middle). The top spectra depict W3 at progressive stages as the protein approaches the T state following photolysis of HbCO. The band envelopes and the difference spectra shown are actually the calculated spectra superimposed on the respective experimental spectra. The frequencies are those of the deconvolved bands; widths and intensities are given in Table I.

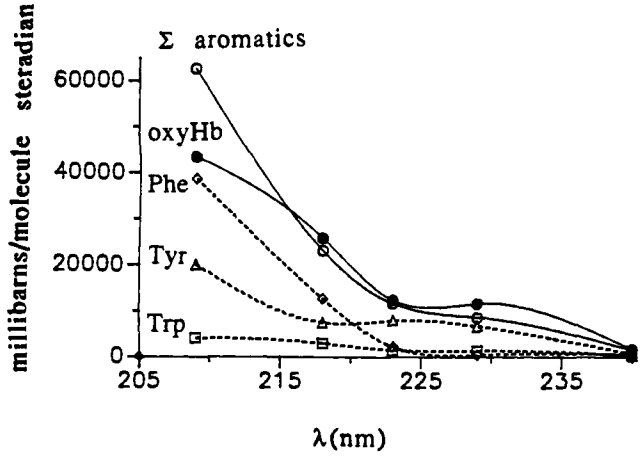

Figure 7. Integrated intensity of the oxyHb 1615/1600-cm^{-1} envelope (●) measured against the 981-cm^{-1} band of sulfate internal standard and expressed in units of cross section.[34] Shown for comparison are the expected intensities[39] (areas) for the ν_{8a} and ν_{8b} bands of Phe (◇) and Tyr (△), as well as the W1 band of Trp (□) from the aqueous solution intensities of the amino acids[33] at the molar concentration of the Hb residues. The sum of these aqueous aromatic amino acid intensities (○) is also plotted for comparison with Hb. For 230-nm excitation, Tyr is the dominant contributor. The curves that connect the points were obtained via cubic spline fit of the data points and are not necessarily intended to imply the actual cross section between data points.

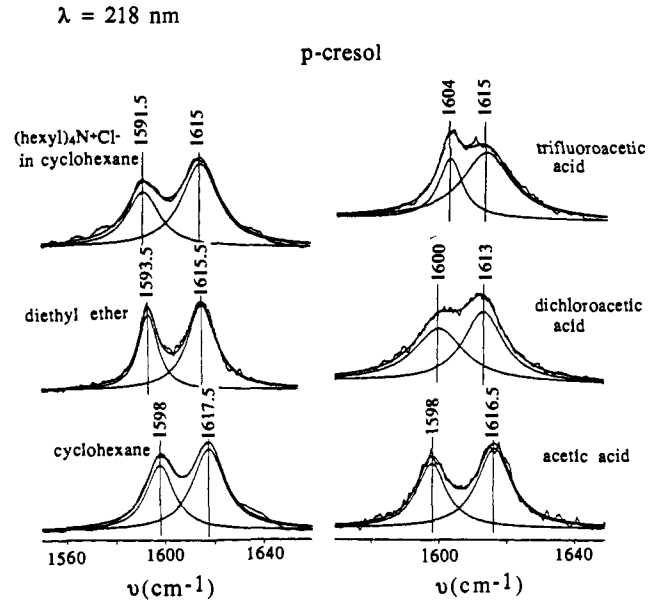

Figure 8. 218-nm excited ν_{8a} and ν_{8b} UVRR bands of *p*-cresol dissolved (2 mM) in the indicated solvents. The smooth curves are the result of spectral deconvolution.

overall Phe scattering in Hb is indicated at this wavelength. At 230 nm, Tyr accounts for almost all of the total intensity. We, therefore, conclude that the RR difference signal in the 1615/1600-cm^{-1} RR bands is primarily due to changes in Tyr environments between deoxyHb and HbCO.

B. Estimation of Environmental Effects from Model Compounds. 1. *p*-Cresol. To evaluate the energetics of the Y8a and Y8b differences between R- and T-state Hb, we examined H-bonding effects on the RR bands of *p*-cresol, a model compound for the Tyr side chain. In a previous report from this laboratory,[38] the Y8b frequency was found to be linearly related to the enthalpy of association of *p*-cresol with H-bond acceptors. We have reevaluated this relationship with improved data, illustrated in Figure 8, using spectral curve fitting to more accurately determine band centers. The new frequencies are listed in Table II, along with the *p*-cresol O–H stretching frequencies, determined by IR spectroscopy. As shown in Figure 9, the frequencies of ν_{8a}, ν_{8b}, and the O–H stretch correlate linearly with the association enthalpy for the three H-bond acceptors (acetone, diethyl ether, and triethylamine) for which enthalpy values have been reported.[39] An additional point is included for tetrahexylammonium chloride dissolved in cyclohexane by interpolating the enthalpy value estimated from the ν_{8b} frequency plot. The chloride ion in cyclohexane, which models H-bonding to an anion, is nearly as strong an H-bond acceptor as is triethylamine. Both have ν_{8b} frequencies close to the 1592-cm^{-1} frequency reported for a protein, OMCHI3, which has a Tyr residue H-bonded to an Asp carboxylate side chain.[39] The linear relationships shown in Figure 9 are represented

Table II. *p*-Cresol ν_{8a} and ν_{8b} Frequencies

solvent	ν_{8b}[a]	ν_{8a}[a]	ν_{OH}[b]	$-\Delta H$[c]	pK_a[d]	λ_{max} (nm)
			Aprotic Solvents			
cyclohexane	1598.0	1617.5	3619	0.0		220
acetone	1595.5	1616.0	3429	4.3		224
diethyl ether	1593.5	1615.5	3348	5.5		228
$N(C_6H_{13})_4Cl$	1591.5	1615.0	3132	7.6[e]		
triethylamine[f]	1590.5	1615.0	3119	8.4		
			Acids			
acetic	1598.0	1616.5			4.75	
chloroacetic	1598.5	1616.0			2.85	
dichloroacetic	1600.0	1613.0			1.29	
trifluoroacetic	1604.5	1615.0			0.24	

[a] Obtained by band deconvolution of 218-nm UVRR spectra as illustrated in Figure 8. [b] From FTIR spectra. [c] Reference 38a–c. [d] Reference 40. [e] Value calculated from the ν_{8b} frequency and the regression line for ν_{8b} in Figure 9. [f] ν_{8a} and ν_{8b} frequencies obtained from 488-nm excited Raman spectrum because triethylamine absorbs strongly at 230 nm.

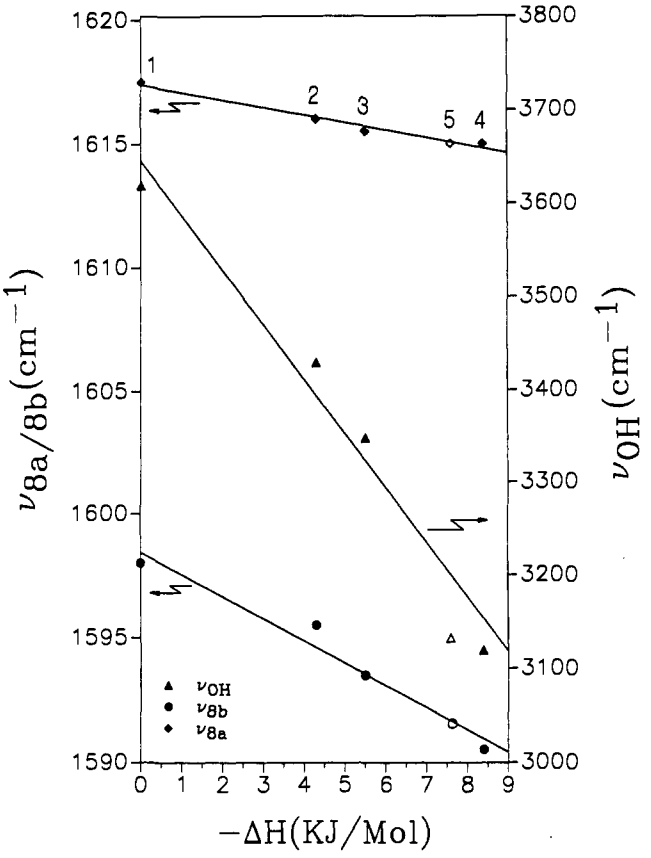

Figure 9. Plots of ν_{8a} (◆), ν_{8b} (●), and ν_{OH} (▲) frequencies for *p*-cresol against its association enthalpy with: (1) cyclohexane, which provides the reference zero for the ΔH scale, (2) acetone, (3) diethyl ether, and (4) triethylamine. The open symbols, labeled 5, are for tetrahexylammonium chloride in cyclohexane, for which the enthalpy is unknown. Its association enthalpy was obtained from the least-squares line through the ν_{8b} data.

by the following empirical equations relating the frequencies (cm^{-1}) and enthalpies (kcal/mol).

$$\nu_{8b} = 1598.5 - 0.94(-\Delta H)$$

$$\nu_{8a} = 1617.4 - 0.31(-\Delta H)$$

$$\nu_{OH} = 3645.0 - 58.5(-\Delta H)$$

The previously reported coefficients of the ν_{8b} equation[39] differ from the present ones mainly because of an inaccurate determination of the reference value in cyclohexane, due to marginal S/N. Care was taken in both studies to dilute the *p*-cresol sufficiently (2 mM) to avoid self-association[40] in cyclohexane; at higher concentrations (75 and 300 mM), self-association was observed to produce a slight upshift (1 cm^{-1}) and significant broadening of ν_{8b}.

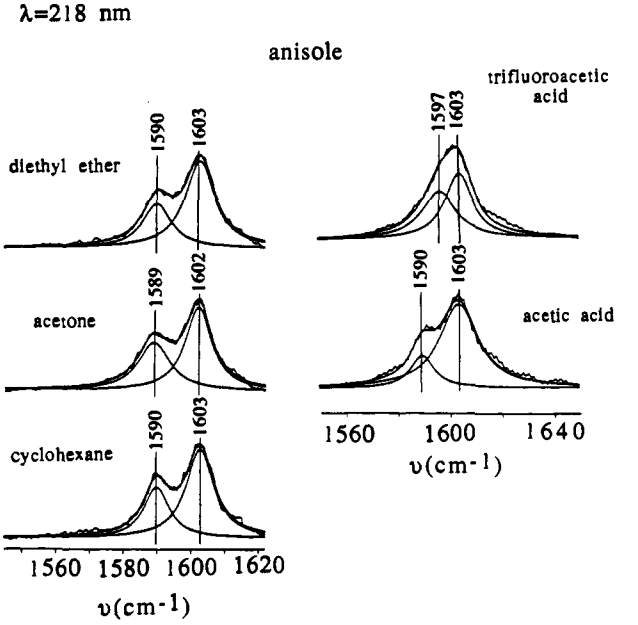

Figure 10. 218-nm excited ν_{8a} and ν_{8b} UVRR bands of anisole dissolved (2 mM) in the indicated solvents. The smooth curves are the result of spectral deconvolution.

As the Tyr-OH can act as a H-bond donor *or* acceptor in proteins,[23] we examined the effect of H-bond acceptance by dissolving *p*-cresol in acidic solvents: acetic, chloroacetic, dichloroacetic, and trifluoroacetic acids. The RR spectra (Figure 8) show a significant upshift of ν_{8b} for the stronger acids. The variation in ν_{8a} is slight, but the band becomes quite broad in the stronger acids, suggesting some environmental heterogeneity. Association enthalpies are unavailable for *p*-cresol with these acids, and their IR absorptions obscure the *p*-cresol O–H stretch. It is clear, however, that trifluoroacetic acid, which has the lowest pK_a (Table II), produces the highest-frequency ν_{8b}.

Figure 10 shows ν_{8a} and ν_{8b} RR bands of anisole, run as a control. The *p*-cresol OH proton is replaced by a methyl group in anisole, which is therefore unable to donate an H-bond. The frequencies are seen to be unaffected in acetone and ether, relative to cyclohexane. This shows that the downshifts observed for *p*-cresol in these solvents are indeed due to H-bond donation. Anisole can, however, accept an H-bond and the ν_{8b} frequency is seen to shift up in trifluoroacetic acid, just as it does for *p*-cresol.

H-bonding also affects the ν_{8a} and ν_{8b} intensities through shifts in the excitation profiles (EP's). Figure 11 shows EP's in cyclohexane, using the 1442-cm^{-1} cyclohexane band as a secondary internal intensity standard.[42] The ν_{8a} EP maximum is at ca. 223 nm in cyclohexane, but shifts to ca. 230 nm when tetrahexylammonium chloride is added, and to ca. 215 nm when trifluoroacetic acid is added. Similar shifts are seen in the position of the L_a absorption band (Table II) and are consistent with the view that the L_a transition has appreciable involvement of oxygen electrons in *p*-cresol or Tyr.[43] The ν_{8b} EP's show a similar trend, but no clear L_a maximum is seen in cyclohexane itself, and the influence of adding trifluoroacetic acid is much smaller than it is for the ν_{8a} profile. These differences may be related to the different scattering mechanisms, vibronic versus Franck–Condon, which are applicable to the ν_{8b} versus ν_{8a} modes.[35] As a result of these EP shifts, the RR intensities at 230 nm are expected to increase when Tyr is an H-bond donor, and decrease when it is an H-bond acceptor, although the effect of H-bond acceptance is smaller for the ν_{8b} than for the ν_{8a} intensity.

On the basis of these model studies, the small upshifts in the Y8a and Y8b bands upon the R→T switch, as well as the intensity decrease of the Y8a band, imply decreased H-bond donation or

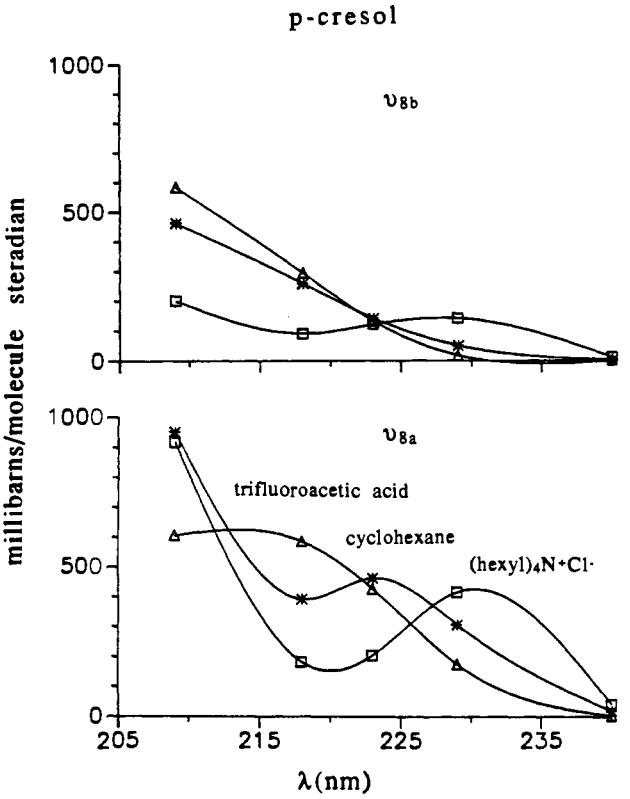

Figure 11. Excitation profiles for ν_{8b} and ν_{8a} bands of *p*-cresol in trifluoroacetic acid (△), cyclohexane (*), and tetrahexylammonium chloride in cyclohexane (□). Band area intensities are given in units of cross section, using the 1442-cm^{-1} cyclohexane band as a secondary internal reference.[41] The curves that connect the points were obtained via a cubic spline fit of the data points and are not necessarily intended to imply the actual cross section between points.

Table III. 3-Methylindole W3 Frequencies and Bandwidths (cm^{-1}) and Absorption Maxima in Various Solvents

solvent	W3	width	DN[a]	AN[a]	λ_{max} (nm)
cyclohexane	1563.0	9.7	0.0	0.0	222
toluene	1561.0	7.9	0.1	8.2	
acetic acid	1559.5	10.2		52.9	
diethyl ether	1559.0	10.8	19.9	3.9	
cyclohexanol	1558.0	10.7			228
ethanol	1558.0	10.8		37.1	
methanol	1558.0	12.3		41.3	224
acetonitrile	1558.0	11.2	14.1	18.9	
acetone	1558.0	10.1	17.0	12.5	
triethylamine	1557.5	11.1	61.0		
H_2O	1556.5	11.0	33.0	54.8	

[a] DN = donor number; AN = acceptor number.[44]

increased H-bond acceptance by one or more of the Tyr residues in deoxyHb.

2. 3-Methylindole. Trp W3 environmental effects were explored with the model compound 3-methylindole (3-MeIn). Miura et al.[44] reported an absence of H-bond sensitivity for W3, but we found the frequency to be somewhat solvent sensitive. As seen in Table III, there is an 8-cm^{-1} spread of frequencies in solvents ranging from cyclohexane to water, but there is no consistent correlation with donor number[45] (DN) of the solvent, a measure of H-bond acceptor strength, or with the acceptor number[45] (AN), a measure of Lewis acidity. Strong donor or acceptor solvents both shift W3 down. This behavior suggests that Lewis acid solvents may interact with the π cloud of the indole ring, while basic solvents interact with the N–H proton, both interactions

(44) Miura, T.; Takeuchi, H.; Harada, I. *J. Raman Spectrosc.* **1989**, *20*, 667.
(45) Gutman, V. *Coord. Chem. Rev.* **1976**, *18*, 225.

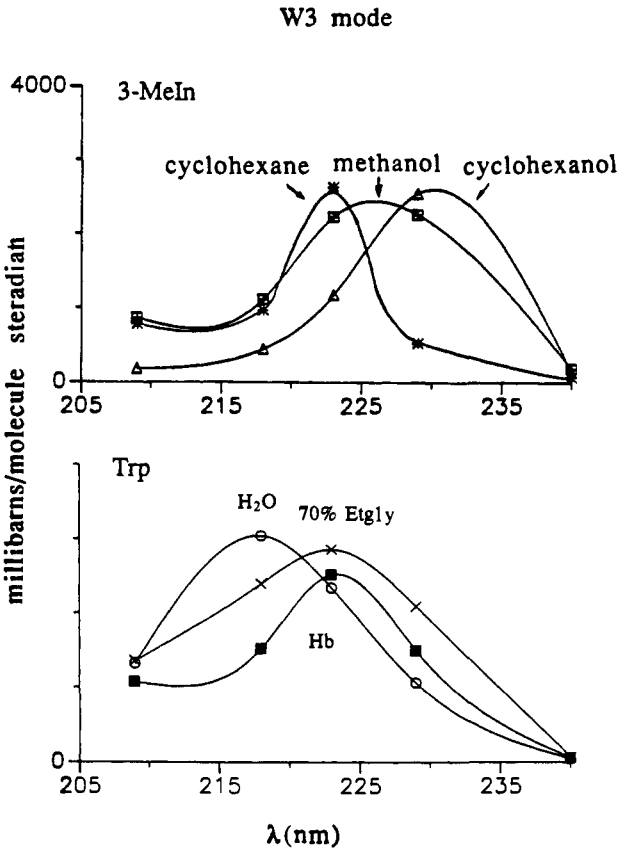

Figure 12. (Top) Excitation profiles for the W3 band of 3-methylindole in the indicated solvents. Band areas were measured versus solvent bands as secondary standards.[41] (Bottom) Excitation profiles for the W3 bands of tryptophan in water (○) and 70% ethylene glycol/water (X), and of the W3 envelope for oxyHb (■). All areas are referenced to the 981-cm^{-1} band of sulfate.[34] The curves that connect the points were obtained via a cubic spline fit of the data points and are not necessarily intended to imply the actual cross section between points.

weakening the ring bonds slightly.

Larger changes are seen in the W3 intensity due to substantial environmental sensitivity of the resonant electronic transition as reflected in the W3 EP. Figure 12 shows that there is a progressive red-shift in the EP maximum for 3-MeIn in cyclohexane, methanol, and cyclohexanol from ca. 223 to 226 to 230 nm. These wavelengths are in reasonable accord with the absorption band maxima of the same solutions (Table III). The red-shift in methanol and the further red-shift in cyclohexanol must reflect the effect of a less polar solvent, superimposed on the H-bond effect. A strongly red-shifted (230 nm) W3 EP has previously been found for horse-heart cytochrome *c*,[27] in which the single Trp residue is strongly H-bonded to a heme propionate group, and is otherwise surrounded by hydrophobic residues. Also, shown in Figure 12 is the EP of Trp in aqueous solution and in 70% ethylene glycol, as well as the EP for the total intensity of the 1555-cm^{-1} band of oxyHb. This last EP coincides rather closely with that of Trp in 70% ethylene glycol and suggests that this solvent is a satisfactory mimic of the average protein environment, as has been found for other proteins.[38]

The large increase in the W3 intensity of Trp β37 between oxy- and deoxyHb with 230-nm excitation (Table I) indicates that it becomes more strongly H-bonded, and/or that the environment becomes more hydrophobic.

C. Time-Resolved Spectra. The Tyr and Trp UVRR bands were employed as monitors of protein structural transients by photolyzing HbCO with a 419-nm laser pulse and probing the photoproduct with an electronically delayed 230-nm Raman excitation pulse as described in the Experimental Section. The violet pulse energy was sufficient to achieve a steady state concentration of deoxyHb in equilibrium with geminately recombined HbCO during the 7-ns laser pulse. This was established by monitoring

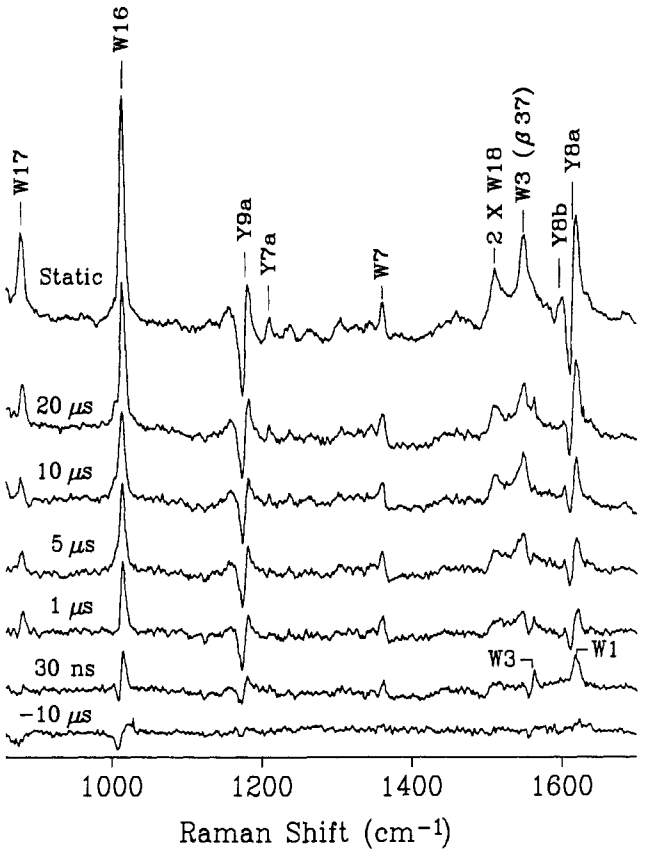

Figure 13. 230-nm excited UVRR difference spectra of photoproduct minus HbCO (no photolysis pulse) at the indicated delay times following photolysis of HbCO with a 419-nm pump pulse. The top spectrum is the same static deoxyHb–HbCO spectrum shown in Figure 1, but plotted on the same scale as the time-resolved spectra. The transient spectra do not reach the intensity of the static spectrum due to second-order CO recombination. See text for discussion of assignments.

the heme RR spectrum generated by the photolysis pulse itself. The heme ν_4 RR band[46] was characteristic of deoxyHb, and showed only a small heme–CO contribution due to geminate recombination[47] during the 7-ns pulse.

The results of the pump–probe experiments are shown in Figure 13. The UVRR spectrum of HbCO, obtained with the same apparatus but without the photolysis pulse, was subtracted from the spectrum of the photolysis mixture at each delay, to generate a series of photoproduct minus HbCO difference spectra. The deoxyHb and phototransient spectra at all time delays were normalized as described for the static difference spectra, so that regardless of the total detector counts for any given spectrum, the intensities of all bands in all of the spectra, including the corresponding difference spectra, could be directly compared with one another.

The difference spectra in Figure 13 exhibit several interesting features and trends. The difference spectrum for a probe-before-pump (time delay of −10 μs) experiment is virtually featureless. The small inflection at the strongest band, W16, reflects the intrinsic uncertainty in the spectral subtraction procedure. In contrast to the −10-μs spectrum, the difference spectrum at 30 ns shows definite and reproducible features. Although earlier transient UVRR difference spectra were reported to be featureless at time delays less than 1 μs,[28] our improved spectral quality in the present experiment establishes that there *are* prompt changes in the UVRR spectrum following photoejection of CO from the heme–CO complex. Moreover, these changes give rise to difference features that are quite distinct from those observed on the microsecond scale. The 30-ns spectrum shows no signal for W17 and derivative shaped signals at the position of W16 and W3, in contrast to the positive-going signals seen in the microsecond regime. Furthermore, the strong derivative signal seen at later times for Y8a is replaced by a positive signal at 30 ns. This positive signal peaks at 1620 cm^{-1}, which is too high a frequency to be associated with the Tyr Y8a mode observed on the microsecond time scale. It is, however, exactly the frequency expected for the Trp W1 mode.[32] We tentatively assign this prompt signal to intensification of the Trp W1 band in the photoproduct, although some contribution from Tyr Y8a is likely, as a small Tyr signal is also seen for Y9a at 30 ns. However, the 30-ns difference spectrum is primarily attributable to Trp alterations that are different from those observed on the microsecond time scale.

The W3 difference signals are key to understanding these prompt changes. When the W3 envelope of the 30-ns photoproduct is subjected to curve-fitting analysis (Figure 6 and Table I), the derivative-shaped difference signal is seen to result from a 0.7-cm^{-1} upshift in the Trp α14 and β15 contribution, whereas the Trp β37 contribution to the difference spectrum is very small. Thus, the prompt change is primarily associated with the Trp α14 and/or β15 residues. We infer that the other prompt features, including the intensification of W1, the upshift in W16, and the absence of a W17 signal, are also associated with environmental changes of Trp α14 and/or β15. From 1 μs onward, the difference spectra evolve toward the static deoxyHb minus HbCO difference spectrum. The evolution is not entirely monotonic, however, as can be seen from the W3 curve-fitting analysis (Table I). The prompt shift in the Trp α14/β15 band remains constant at +0.7 cm^{-1} from 30 ns to 20 μs, but relaxes back slightly in the static difference spectrum (+0.3 cm^{-1}). Meanwhile the Trp β37 band intensity increases strongly between 1 and 10 μs, almost to the deoxyHb intensity, but at 20 μs it drops back to about the intensity seen at 5 μs. We interpret this drop in difference band intensity at 20 μs to second-order recombination with CO in solution. The recombination rate is significant on the tens-of-μs time scale,[9,10] even though the partial pressure of CO over the solution is only ~75 mmHg. Under 1 atm CO pressure, the rate of second-order heme–CO recombination was competitive with the rate of the quaternary R→T switch. Consequently, the difference spectrum (data not shown) could not evolve past the 1-μs spectrum that is shown in Figure 13. The 20-μs spectrum clearly contains a difference feature, whose origin is not clear, at the frequency of the prompt Trp α14/β15 signal. The feature occurs with a simultaneous upshift of the W16 difference signal, which otherwise shows a monotonic shift to lower frequency through the R→T transition (Figure 14). Since these additional 20-μs features resemble those seen in the 30-ns spectrum, a possible explanation is that partially ligated HbCO, which is the result of CO recombination, is photolyzed by the UV Raman excitation pulse with a quantum efficiency higher than that exhibited by R-state HbCO. This interpretation is consistent with the 2-fold greater quantum efficiency for CO photolysis in the T state over that in the R state.[9,10] Alternatively, an additional tertiary intermediate, resembling the 30-ns intermediate, builds up at 20 μs.

The 1-μs difference spectrum is not simply an attenuated copy of the static difference spectrum, but shows qualitatively different features. This is especially clear for the W17 difference peak, which is absent at 30 ns and is comprised of two components between 1 μs and 20 μs (882.4 and 878.6 cm^{-1}). Figure 14 shows that at 1 μs the 882.4-cm^{-1} component dominates the W17 difference feature. Between 1 and 10 μs the 882.4-cm^{-1} difference band decreases in intensity with a simultaneous intensity increase in the 878.6-cm^{-1} component. As with the Trp α14/β15 W3 difference intensity and the W16 frequency, there is a discontinuity in the trend of the relative intensities of the W17 components at 20 μs. We postulate that the reintensification of the 882.4-cm^{-1} component is explained by the photolysis of partially ligated T-state hemoglobin arising from second-order recombination. Hence, the spectra provide clear evidence for a different intermediate protein structure on the microsecond time scale than the prompt inter-

(46) Spiro, T. G.; Li, X.-Y. In *Biological Applications of Raman Spectroscopy*; John Wiley: New York, 1988; Vol. 3, pp 1–38.
(47) Lyons, K. B.; Friedman, J. M. In *Hemoglobin and Oxygen Binding*; Ho, C., Ed.; Elsevier Biomedical: Amsterdam, 1980; pp 333–338.

Table IV. Trp H-Bonding in Hb[a]

residue	oxyHb H-bond acceptor	oxyHb NH···X (Å)	oxyHb ∠N-H-X (deg)	deoxyHb H-bond acceptor	deoxyHb NH···X (Å)	deoxyHb ∠N-H-X (deg)
Trp α14[b]	Thr α67(OH)	1.6	172	Thr α67(OH)	1.8	172
Trp β15[b]	Ser β72(OH)	2.4	160	Ser β72(OH)	1.9	139
Trp β37	Asn β102(CO)	1.9	164	Asp α94(COO^-)	2.0	158

[a] Distances and angles calculated from X-ray coordinates[44,45] after placing H 1.03 Å from the indole N, along the line bisecting the C-N-C angle. [b] The H-bond changes are connected with displacements of the A and E helices between the oxy and deoxy structures, from a 9.4-Å separation of backbone C atoms (of Trp α14 and Thr α67) in oxy to 8.8 Å in deoxy for the α subunit, and from 9.5 Å (Trp β37-Ser β72) to 9.1 Å in the β subunit.

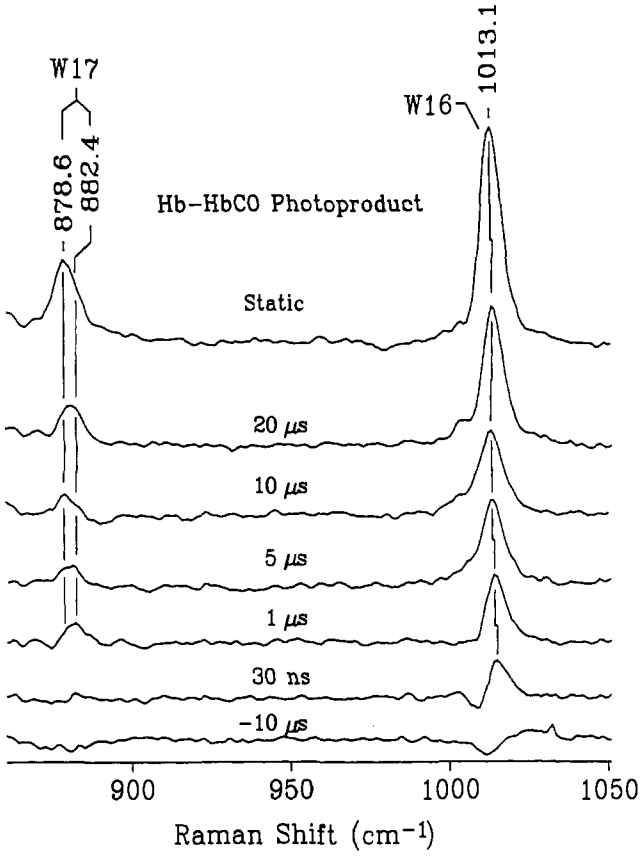

Figure 14. Expanded view of the low-frequency region of Figure 13 showing the time-dependent shifts of the W16 difference band and the changes in the spectral inhomogeneity of the W17 difference feature as a function of time.

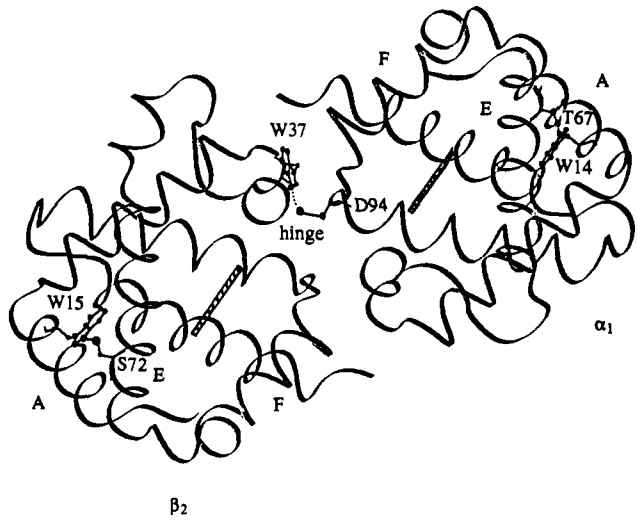

Figure 15. Ribbon diagram of the α_1 and β_2 subunits of deoxyHb, showing the Trp β37-Asp α94 interaction at the "hinge" or "flexible joint" of the $\alpha_1\beta_2$ interface. The Trp β15-Ser β72 and Trp α14-Ser α67 interaction between the A and E helices of each subunit are also depicted. The heme groups, seen nearly on edge, are indicated by the hashed bars.

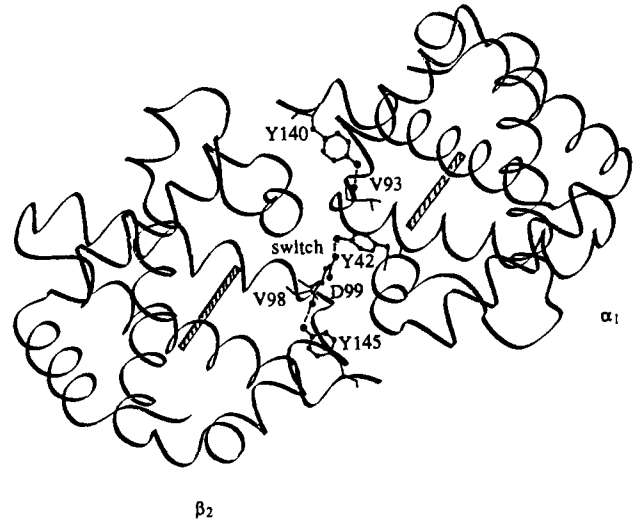

Figure 16. Ribbon diagram, as in Figure 15, but showing the Tyr α42-Asp β99 interaction in the "switch" region of the $\alpha_1\beta_2$ interface. The Tyr α140-Val α93 and Tyr β145-Val β98 interactions are also depicted. The remaining Tyr residues have no H-bond partners and have been omitted for clarity.

mediate or final deoxyHb structures.

Discussion

To interpret the UVRR results, we examined the environments of the aromatic residues in single crystals based on X-ray crystallographic coordinates for oxy-[48] and deoxyHb[49] (available in the Brookhaven crystallographic data bank). Figures 15 and 16 show ribbon diagrams of the $\alpha_1\beta_2$ subunit pair for oxyHb, in the same orientation chosen by Baldwin and Chothia,[6] to illustrate the critical interactions involved in the transition between the R and T quaternary structures. Figure 15 shows the Trp residues and their H-bond partners, whereas Figure 16 shows those Tyr residues known to have H-bond partners. Three other Tyr residues (α24, α35, and β130) are omitted for clarity. They have no H-bond partners in either oxy- or deoxyHb, and their environments are not significantly altered by the R→T transition. Consequently, they are assumed not to contribute to the R→T UVRR difference signals.

The two inter-subunit contact regions that show most of the alterations are between the C helix of α_1 and the FG corner of β_2, and between the C helix of β_2 and the FG corner of α_1. The former contact was called the "switch" by Baldwin and Chothia,[6] because this region of the subunit interface undergoes a wholesale offset of the side-chain interdigitation between the two subunits as a H-bond involving Tyr α42 is formed or broken. The latter contact was designated as the "hinge" or "flexible joint", because it supports the swiveling of the interface, with some reorientation of the side chains, but no significant translation. Although the inter-subunit H-bond involving Trp β37 at the hinge is broken to form an *intra*-subunit H-bond, the hinge contact is maintained via several other H-bonds, salt bridges, and nonbonding inter-

(48) Shaanan, B. *J. Mol. Biol.* **1983**, *171*, 31.
(49) Perutz, M. F.; Hasnain, S. S.; Dukl, P. J.; Sessler, J. L.; Hahn, J. E. *Nature* **1982**, *295*, 535.

Table V. Tyr H-Bonding in Hb[a,b]

	oxyHb			deoxyHb		
residue	H-bond acceptor	OH···X (Å)	∠O–H–X (deg)	H-bond acceptor	OH···X (Å)	∠O–H–X (deg)
Tyr α140	Val α93(CO)	1.6	174	Val α93(CO)	1.7	155
Tyr β145	Val β98(CO)	1.5	155	Val β98(CO)	1.6	170
Tyr α42	none			Asp β99(COO^-)	1.6	162
				{(COOH)	1.5	161}

[a] Distances and angles calculated from X-ray coordinates after placing H 1.03 Å from the Tyr–O atom with ∠C–O–H = 120°, and allowing the C–OH bond to swivel and find an optimum geometry. [b] Interior Tyr residues α24 (B helix), β130 (H helix), and β35 (C helix at $\alpha_1\beta_1$ interface) lack H-bonds in both forms.

Table VI. Trp Residue $\chi^{2,1}$ Angles (deg)[a] and W3 Frequencies (cm^{-1})

	Trp β37			Trp β15			Trp α14		
quaternary state	W3 $\chi^{2,1}$	W3 pred[b]	exp[c]	W3 $\chi^{2,1}$	W3 pred[b]	exp[c]	W3 $\chi^{2,1}$	W3 pred[b]	exp[c]
oxyHb	92	1549	1547.1	115	1557	1557.9	122	1558	1557.9
deoxyHb	93	1550	1548.2	104	1554	1558.3	100	1553	1558.3
oxy-deoxy	−1	+1	+1.1	+9	−3	+0.4	+22	−5	+0.4

[a] Calculated from the coordinates[44,45] in the Brookhaven data bank. [b] Predicted from the correlation of Muira et al.[39] [c] Experimental values obtained from deconvoluted UVRR bands with peak-picking uncertainty of ±0.1 cm^{-1}. The same frequencies are listed for Trp α14 and β15, both of which contribute to a single deconvoluted band.

actions.[6] It should be noted that a symmetry-related pair of contacts is found at the $\alpha_2\beta_1$ interface. The two other Trp residues, α14 and β15, are interior residues and are located on the A helices of the respective chains. The indole rings of these residues bridge to the E helices by donating H-bonds to the OH groups of Thr α67 and Ser β72, respectively. The other two H-bonded residues, Tyr α140 and Tyr β145, are at the C-termini and are near the $\alpha_1\beta_2$ interface, but their H-bond partners, the carbonyl groups of Val α93 and Val β98, are at the FG corners of their own chains. Details of the H-bonding in the R and T states are given in Tables IV and V and are discussed below.

A. Trp Environments and the Spectral Response. In an effort to understand the Trp W3 difference features and their temporal evolution, we apply the correlation recently reported by Miura et al.[44] between the W3 frequency and a series of crystalline Trp derivatives that exhibit variations in the dihedral angle, $\chi^{2,1}$, about the bond connecting the indole ring with the C_β atom of the Trp side chain. A monotonic increase of the W3 frequency with $\chi^{2,1}$ was found for angles between 60° and 120°. This variation is believed to involve an electronic effect that alters the bonding in the indole ring.[44] In Table VI, we list the $\chi^{2,1}$ angle calculated for the three Trp residues from the crystal structure coordinates for oxy- and deoxyHb. Also listed are the W3 frequencies expected on the basis of the $\chi^{2,1}$ correlation and the frequencies of the deconvoluted W3 components. The correspondence between the predicted and experimental frequency is striking. It is particularly gratifying that the W3 component, which has been assigned independently to Trp β37 on the basis of the Hb Rothschild spectrum, is correctly predicted to have the lowest frequency, as it has the lowest $\chi^{2,1}$ angle. Thus, nature has greatly aided the spectroscopic analysis by shifting the $\chi^{2,1}$ angle and therefore the W3 frequency, to a distinguishable value for the critical Trp β37 residue.

There are, however, small discrepancies between predicted and experimental frequencies, seen most clearly in the deoxyHb–HbCO differences. Whereas the predicted and observed differences are +1 and +1.1 cm^{-1}, respectively, for Trp β37, the predicted differences are −3 and −5 cm^{-1} for Trp β15 and Trp α14, respectively. The maximum of the deconvoluted peak that encompasses both of these bands is observed to shift only by ~0.4 cm^{-1} in concert with a 4% decrease in intensity. These changes give rise to the small shoulder on the high-frequency side of the Trp β37 difference signal. The discrepancies between predicted and experimental W3 frequencies are attributed to the convolution of more than one environmental perturbation as follows.

The H-bond partners of the three Trp residues are listed in Table IV, along with the N–H···X distances and angles calculated from crystal structure coordinates; H atoms were inserted at a standard distance of 1.03 Å along the line bisecting the indole C–N–C angle. As noted above, Trp α14 and Trp β15 connect the A and E helices; the H-bonds to Tyr α67 and Ser β72 are present in both structures, but their geometries change slightly as a result of shifts in the helix positions. In oxyHb the Trp α14 H-bond distance of 1.6 Å and angle of 172° are both favorable for H-bonding, but in deoxyHb the distance is calculated to increase by 0.2 Å. For Trp β15, the crystal structure coordinates reveal poor H-bond geometries in both R- and T-state Hb. The distance is long, particularly in oxyHb (2.4 Å), and the angle is unfavorable, especially in deoxyHb. It is possible that the downshift expected on the basis of the $\chi^{2,1}$ change is overbalanced by weakening of the H-bonds in deoxyHb, as the 3-MeIn data indicate that W3 shifts down when Trp is an H-bond donor. However, the absence of a W17 *shift* attributable to Trp α14 and β15 (see below) suggests that other factors are responsible for the change, since the W17 frequency is sensitive to H-bonding.[23]

In oxyHb the H-bond acceptor for Trp β37 is the backbone carbonyl oxygen of Asn β102 in the same subunit, whereas in deoxyHb the acceptor is the Asp α94 carboxylate group across the $\alpha_1\beta_2$ subunit interface. The calculated N–H···O distances are somewhat long in both cases (1.9 and 2.0 Å), but the angles (164° and 158°) are reasonable. The Asp α94 is assumed to be deprotonated, as there are two resolved water molecules nearby (2.8 and 2.9 Å). The H-bond to the negatively charged carboxylate moiety is expected to be stronger than that to the neutral peptide carbonyl in oxyHb. In light of the H-bonding sensitivity of the 3-MeIn EP (Figure 12), a stronger H-bond would explain the 37% increase in the W3 intensity for Trp β37 in deoxyHb. Nevertheless, a stronger H-bond in deoxyHb is thrown into question by the unshifted frequency of W17, a mode that is known[23] to shift down when Trp is an H-bond donor. Kaminaka et al.,[29] however, do report an upshift for W17 in the CO-phototransient spectra with 217.8-nm excitation, and this issue remains to be resolved by further experiments. In view of the sensitivity of the W3 EP to hydrophobic influences (Figure 12), other changes in the Trp β37 environment could account for some of the W3 intensity change. In particular, nonbonding interactions with Asp α94 and Pro α95 are maintained in both the R and T states, while a nonbonding interaction with Tyr α140 exists in the deoxyHb but is absent in oxyHb.[6]

B. Trp W3 and W1 Monitor Tertiary As Well As Quaternary Changes. The optical transient studies of Hofrichter et al.[9] have revealed time constants of ca. 0.1, 1.0, and 20 μs in the heme absorption amplitudes following heme–CO photolysis under conditions similar to those in the present experiment. Our 30-ns time slice precedes the first of these transients and therefore samples the protein before any relaxation (beyond the initial photodissociation process) is detectable at the heme. The absence of any W3 change arising from Trp β37 in the 30-ns difference spectrum implies that the Trp β37 residue, at the "hinge" region of the $\alpha_1\beta_2$ interface, does not sense any structural alteration in

this unrelaxed state, which we label Hb^0.

The prompt W3 difference signal seen for Trp α14 and β15, however, indicates that these residues do register a structural alteration in Hb^0. Both indole rings span the A and E helices of the α and β subunits at essentially equivalent positions by similar H-bonds to Thr and Ser OH groups. The E helices line the distal side of the heme pockets in both subunits, and are plausibly involved in the initial protein structural adjustment to ligand dissociation. The Trp α14 and β15 indole rings act as sensors to this adjustment. As the prompt 0.7-cm^{-1} upshift in the Trp α14/β15 W3 frequency is twice that of the deoxyHb–HbCO frequency difference, the indole sensors are reporting a larger structural change involving the E helix for Hb^0 than for the final T state. This larger change may result from forces generated in the vicinity of the heme that are required for the protein to overcome a tertiary activation barrier along the R→T reaction coordinate. While it is tempting to suppose that the indole sensors respond to changes in the inter-helical H-bonds, the absence of any prompt difference signal for the W17 mode, an H-bonding marker, indicates that other environmental factors are responsible for the 30-ns difference spectrum. These factors produce an upshift in W16, as well as W3, and an intensification of W1 (Figure 3).

The 1-μs time slice corresponds to the time constant for the transition between the first and second stages of protein relaxation, Hb^1 and Hb^2, as reflected in the heme optical spectra.[9] The Trp α14/β15 W3 parameters are identical with those found at 30 ns (Table I), but the Trp β37 W3 band shows a 10% intensity increase. In addition, a W17 difference signal is seen (Figure 14) whose peak frequency is 3.8 cm^{-1} *higher* than the static difference frequency (882.4 cm^{-1} at 1 μs and 878.6 cm^{-1} for static difference). As the W17 frequency is expected to decrease when Trp is a H-bond donor,[23] this behavior suggests that the Trp β37 H-bond seen in the T state is weakened in Hb^1 and/or Hb^2 prior to the establishment of the T-state H-bond. Thus, the W17 difference signal may reflect an intermediate protein structure in which Trp β37 is between its R- and T-state H-bond acceptors.

The 5-, 10-, and 20-μs difference spectra monitor the transition from Hb^2 to the equilibrium deoxyHb structure, Hb^T. Although the 20-μs spectrum deviates from the trend toward the T-state spectrum due to heme–CO recombination effects, the data are consistent with a steady evolution of the Trp β37 W3 band toward its T-state parameters, and with a relaxation of the Trp α14/β15 W3 frequency shift. The other bands in the spectra likewise appear to undergo a continuous evolution, although the data have not yet been analyzed quantitatively.

C. The Tyr Response and Environment; Is Asp β99 Protonated? Of the six inequivalent Tyr residues, three experience insignificant environmental changes between oxy- and deoxyHb. Tyr α24 and Tyr β130 are interior residues (B and H helices), and Tyr α35 is at the $\alpha_1\beta_1$ interface, which is thought to remain unaltered during the inter-dimer rotation of the R→T transition.[6] The residue neighbors are the same, and there are no potential H-bond donors or acceptors in either structure.

The remaining three Tyr residues are at the $\alpha_1\beta_2$ interface. Tyr α140 and Tyr β145 are near the C-termini and donate H-bonds to backbone carbonyl groups of their own chains (Val α93 and Val β98, respectively). The O–H···O distances and angles are favorable and are nearly the same in oxy- and deoxyHb (Table V). Consequently, it seems unlikely that Tyr α140 and Tyr β145 are important contributors to the UVRR difference signals. We note that both of these Tyr residues were initially believed to be mobile in oxyHb on the basis of the electron density maps,[6] but they are well located in a subsequent high-resolution structure.[48] Nevertheless, the possibility of a contribution from Tyr α140 cannot be completely ruled out, as it gains a nonbonding interaction with Trp β37 upon the R→T transition. Insofar as this could cause a shift in the Tyr electronic absorption maximum, with a consequent shift in its EP, Tyr α140 may contribute to the UVRR difference spectrum by means of Raman intensity changes.

Most of the Tyr contributions to the difference spectra grow in at later times, although the Y9a band does show a 30-ns difference feature that seems to be too large to be attributable to the late changes. These late changes, however, grow in monotonically from 1 to 20 μs, and are, therefore, attributable to the Hb^2→Hb^T transition. It seems likely that they are mainly associated with the Tyr α42 residue, which is in the "switch" region of the $\alpha_1\beta_2$ interface, where the major interfacial displacement occurs and the registration of the side chains is completely altered.[6] In deoxyHb the Tyr α42 OH group is in contact with the carboxylate group of Asp β99, while in oxyHb neither Tyr α42 nor Asp β99 has an amino acid H-bond partner. The Tyr α42–Asp β99 interaction is clearly important to the stability of the T state, as cooperativity is significantly reduced when Asp β99 is replaced by other residues in natural mutants,[50-52] or when Tyr α42 is replaced by Phe via genetic engineering.[54]

It has generally been assumed that the interaction involves H-bond donation from the Tyr α42 OH to an ionized carboxylate on Asp β99. However, such an interaction should have produced a UVRR *downshift*, especially in Y8b, as opposed to the observed *upshift*. As noted above, H-bonding of *p*-cresol to tetrahexylammonium chloride in cyclohexane produces a ν_{8b} downshift of 6.5 cm^{-1} (Table II), and similar downshifts have been seen in proteins known to have a Tyr residue H-bonded to a carboxylate.[38] Moreover, H-bond donation should increase the ν_{8b} intensity markedly at 230 nm (Figure 11), so that the expected frequency decrease should be clearly detectable, even against the background of the remaining Tyr residues. Instead, the Y8b band shifts up on the order of 1 or 2 cm^{-1} with little apparent intensity change. At the same time Y8a shifts up by 1.8 cm^{-1} with a 3% loss in intensity (Figure 3). These changes are averaged over all six Tyr residues and are actually larger if attributed to only one of them. This behavior suggests that the Tyr α42 OH acts as a H-bond *acceptor*. In support of this conclusion, we note that ν_{8b} of *p*-cresol shifts up by 6 cm^{-1} in trifluoroacetic acid (Figure 8) while ν_{8a} shows a substantial decrease in intensity with 230-nm excitation (Figure 11).

Examination of the deoxyHb coordinates shows that, while a good Tyr α42 donor H-bond can be formed with Asp β99 carboxylate, an equally good *acceptor* H-bond can be formed by simply swiveling the carboxylate, if the latter is assumed to be protonated. These possibilities are compared in Figure 17, and the calculated H-bond parameters are given in Table V. The Tyr difference signals suggest that Asp β99 is indeed protonated.

We are unaware of any direct evidence regarding the protonation state of Asp β99. Although the pH titration curve of Hb is consistent with normal pK_a's for all carboxylate groups,[55] the curve fitting cannot resolve one or two residues with anomalous pK_a's among the numerous titratable groups. There is a 9.4-ppm (relative to H_2O) ^2H_2O-exchangeable ^1H NMR resonance in deoxyHb, which disappears in the R state.[57] It is not seen when Asp β99 is mutated to Asn (Hb Kempsey) or to His (Hb Yakima) and has, therefore, been assigned to the Tyr α42-Asp β99 H-bond proton. This assignment does not, however, establish whether the proton is donated by the Tyr or the Asp. Examination of the T-state crystallographic coordinates suggests that the Asp β99 carboxylate group might well be protonated since, apart from the Tyr α42 hydroxyl moiety, it is surrounded by hydrophobic groups and the accessible surface area, as measured by the Lee and Richards rolling sphere method,[56] is negligible. Four resolved water molecules are found in the crystal structure within 6 Å of

(50) Weatherall, D. J., et al. *Br. J. Haemotol.* **1977**, *35*, 177.
(51) Bunn, H. F.; Forget, B. G. *Hemoglobin: Molecular Genetic Clinical Aspects*; Saunders: New York, 1980.
(52) Pettigrew, D. W., et al. *Proc. Natl. Acad. Sci. U.S.A.* **1982**, *79*, 1849.
(53) Lindstrom, T. R.; Baldassare, J. J.; Bunn, H. F.; Ho, C. *Biochemistry* **1973**, *12*, 4212.
(54) Nagai, K. *J. Biol. Chem.* **1989**, *264*, 14624.
(55) Janssen, L. H. M.; Bruin, S. H.; Os, G. A. *J. Biochim. Biophys. Acta* **1970**, *221*, 214.
(56) Lee, B.; Richards, F. M. *J. Mol. Biol.* **1971**, *55*, 379.
(57) (a) Fung, L. W.-M.; Ho, C. *Biochemistry* **1975**, *14*, 2526. (b) Viggiano, G.; Wiechelman, K. J.; Chervenick, P. A.; Ho, C. *Biochemistry* **1978**, *7*, 795.
(58) Gao, J.; Kuczera, K.; Tidor, B.; Karplus, M. *Science* **1989**, *244*, 1069.

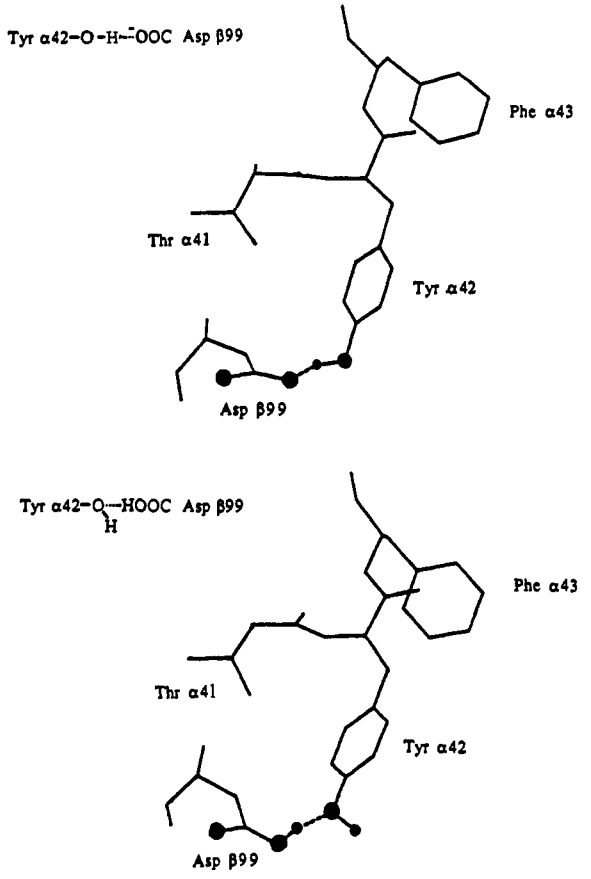

Figure 17. Alternative H-bond possibilities for the Tyr α42–Asp β99 interaction: (top) a donor bond to deprotonated carboxylate, (bottom) an acceptor bond from protonated carboxylate. Both structures are based on the deoxyHb crystal structure coordinates, with rotation of the $-COO^-$ group to allow optimum H-bond geometry.

the Asp β99 carboxylate, but they are all H-bonded to other side chains from Asp α94, Asn β97, and Asn β102, and they are well localized, as indicated by their small *B* values. The closest one is ~3 Å from the Asp β99 carboxylate. The low dielectric constant implied by the hydrophobic environment of Asp β99 suggests an elevated pK_a for this residue.

If the Asp β99 carboxylate group is protonated in the T state, might it contribute to the Bohr effect,[59,60] by giving up its proton on oxygenation? In the R state there is no specific H-bond partner for Asp β99, and solvent accessibility is increased, although not dramatically. The Lee and Richards technique[56] gives a value of 13% for the solvent accessible area of the side chain, and Karplus et al.[58] find two additional water molecules in contact with the carboxylate group in the energy-minimized structure (see below). The Asp β99 pK_a is, therefore, expected to be lower in the R than in the T state, but it is unclear by how much. Ohe and Kajita[61] have shown that a careful inventory of histidine and α-amino contributions does not fully account for the Bohr effect, implying that other residues contribute significantly. The role of Asp β99 therefore remains open.

A quite different inference can be drawn from the energy perturbation calculation by Karplus and co-workers[58] on the mutation involved in Hb Radcliffe,[50] in which Asp β99 is replaced by an alanine residue. In this calculation a spherical zone of the protein encompassing the mutant residue was "carved" out and was subjected to solvation and energy minimization. A number of solvent interactions were found to contribute importantly to the simulated free energy change associated with the mutation. The Asp β99 side chain was found to interact with three water molecules in the T state and with five in the R state. It is important to note, however, that the Asp β99 carboxylate side chain was *assumed* to be deprotonated in both quaternary structures. Given that the solvation profile may depend critically on the system chosen, the notion that the energy minimization procedure of the model system introduced solvent contacts that might not occur if the carboxylate were protonated, cannot be discounted. To resolve this issue computationally, it is necessary to simulate the same system with a protonated Asp β99 residue.

Conclusions

The 230-nm excited UVRR difference spectrum between deoxyHb and HbCO contains several features between 850 and 1700 cm^{-1} that arise from changes in Tyr and Trp vibrational modes. The 1555-cm^{-1} W3 UVRR band is especially informative because it can be resolved into contributions from Trp β37, in the "hinge" region of the $\alpha_1\beta_2$ interface, and from Trp α14 and β15, which are interior residues that bridge the A and E helices via H-bonds at equivalent positions in the α and β subunits. A pump–probe difference spectrum of the HbCO photoproduct obtained 30 ns after photolysis reveals Trp α14/β15 spectral alterations which are attributable to movement of the distal E helices in the unrelaxed protein structure of the prompt photoproduct. The Trp β37 W3 band shows essentially no change, which suggests that the $\alpha_1\beta_2$ interface is unaltered prior to protein relaxation. In the spectrum acquired at 1-μs delay, the Trp α14/β15 W3 band is the same as at 30 ns, whereas the Trp β37 W3 band is altered and a W17 difference band appears at a frequency of 3.8 cm^{-1} higher than that seen in the static difference spectrum. An intermediate protein structure is suggested in which Trp β37 is not H-bonded to its R-state or to its T-state partner. Between 1 μs and 20 μs, the transient difference spectra evolve toward the static difference spectrum, and the features are attributed mainly to the $\alpha_1\beta_2$ interface residues Trp β37 and Tyr α42. The T-state H-bond between Tyr α42 and Asp β99 is proposed to be a Tyr *acceptor* H-bond from protonated Asp-carboxylate rather than a donor H-bond to deprotonated carboxylate, based on the UVRR changes associated with Y8a and Y8b. Asp β99 protonation would be consistent with the hydrophobic character of the Asp β99 environment in the T state, as revealed by the crystal-structure coordinates. This proposal raises the possibility that Asp β99 is involved in the Bohr effect.

Acknowledgment. We thank Professor Gary Ackers for a sample of Hb Rothschild and Professor Martin Karplus for helpful discussions. This work was supported by NIH Grant GM33576 and NRSA fellowship No. 5 F32 HL08116-01 (K.R.R.).

Registry No. $C_4H_7NO_4$, 56-84-8; $CH_3C(O)CH_3$, 67-64-1; EtOEt, 60-29-7; $N(C_6H_{13})_4Cl$, 140175-47-9; $N(Et)_3$, 121-44-8; CH_3CO_2H, 64-19-7; $ClCH_2CO_2H$, 79-11-8; Cl_2CHCO_2H, 79-43-6; F_3CCO_2H, 76-05-1; MeC_6H_5, 108-88-3; c-$C_6H_{11}OH$, 108-93-0; EtOH, 64-17-5; MeOH, 67-56-1; CH_3CN, 75-05-8; carbonyl HbA, 9072-24-6; L-tryptophan, 73-22-3; L-tyrosine, 60-18-4; cyclohexane, 110-82-7; *p*-cresol, 106-44-5; 3-methylindole, 83-34-1.

(59) Perutz, M. F.; Hasnain, S. S.; Dukl, P. J.; Sessler, J. L.; Hahn, J. E. *Nature* **1982**, *295*, 535.
(60) Kilmartin, J. V. *Trends Biochem. Sci.* **1977**, 247.
(61) Ohe, M.; Kajita, A. *Biochemistry* **1980**, *19*, 4443.